Model of thermal conductivity in powder beds

A. V. Gusarov*
ENISE, 58 rue Jean Parot, 42023 Saint-Etienne, France

E. P. Kovalev
IMET, Leninsky Prospekt 49, 119991 Moscow, Russia

(Received 11 March 2009; revised manuscript received 8 June 2009; published 7 July 2009)

Heat transfer between contacting solid particles in gas is localized about the points of contact because of the low thermal conductivity of gas. This suggests the model of a network of discrete thermal resistances. Thermal interaction of two particles in the zone of contact between them includes thermal conductivity in the solid phase as well as heat transfer through a gas gap between the particles, where the conductive heat transfer at higher distances from the center of the contact changes to the transition transfer and free molecular transfer near the contact center. In the framework of this approach the effective thermal conductivity depends on three dimensionless morphological parameters: the volume fraction of solid phase, the mean coordination number, and the ratio of the size of necks between particles to the size of particles. The physical properties of the phases are specified by the thermal conductivities of the solid and the gas, the adiabatic exponent of the gas, and the Knudsen number. The proposed model agrees with the experimental S curves of the effective thermal conductivity versus the logarithm of gas pressure. It also describes the experimental tendencies of increasing the effective thermal conductivity with the particle size and the volume fraction of solid. The model can be applied to powder beds with micron-sized particles as well as to packed beds with millimeter-sized particles in gas. Free molecular and transient regimes of heat transfer in the gas filling pores can be important even for millimeter-sized particles at atmospheric pressure when the Knudsen number is as low as 10^{-5}. These rarefied gas phenomena are responsible for such a complicated behavior of the considered heterogeneous media. Their quantitative description gives the model, which does not contain fitting parameters.

DOI: 10.1103/PhysRevB.80.024202 PACS number(s): 44.30.+v, 44.35.+c

I. INTRODUCTION

Transport processes in heterogeneous media are long explored.[1] Nevertheless, new aspects of this problem are arising due to recent applications.[2,3] This can be explained by a great variety of morphology of heterogeneous structures because each type of morphology often necessitates a special approach. This paper is encouraged by the studies of selective laser sintering/melting of powders,[4] while the application field could be wider.

The powder bed is considered as a multiphase heterogeneous medium with the structure of packed bed, where the solid particles are dispersed in a continuous gas phase in such a way that they touch each other. The dispersed particles can form point contacts between them. The point contacts become the surface ones as a result of mechanical deformation of particles at compacting,[5] sintering at elevated temperatures,[6] or condensing a liquid at high humidity.[7] Thus, the morphology is formed, which will be referred to as the structure of slightly sintered powder bed. The area of the contacts between solid particles is supposed to be much less than the area of the solid gas boundaries, so that the particles can still be distinguished in the slightly sintered structure. Materials with the described structure are widely used for thermal insulation.[8] The same morphology is typical at selective laser sintering of powders.[9]

In 1873 Maxwell proposed the estimate of the effective conductivity λ_e of dispersed medium based on the problem of interaction of a single particle with the matrix[10]

$$\frac{\lambda_e}{\lambda_g} = \left(1 - 2f_s\frac{1-\lambda_s/\lambda_g}{2+\lambda_s/\lambda_g}\right) \Bigg/ \left(1 + f_s\frac{1-\lambda_s/\lambda_g}{2+\lambda_s/\lambda_g}\right), \quad (1)$$

where λ_g is the conductivity of the matrix, λ_s is the conductivity of the dispersed phase (particles), and f_s is the volume fraction of the dispersed phase. This model neglects the mutual influence of the dispersed particles and is rigorous in the limit $f_s \to 0$. In 1935 Bruggeman tried to overcome this restriction by changing the matrix with an effective homogeneous medium with self-consistent conductivity depending on the influence of neighbor particles. This approach gave implicit formula[11]

$$1 - f_s = \frac{\lambda_s - \lambda_e}{\lambda_s - \lambda_g}\left(\frac{\lambda_g}{\lambda_e}\right)^{1/3}. \quad (2)$$

According to more recent estimates[12] Eq. (2) is satisfactory at $f_s < 0.2$, which is considerably less than the typical values of f_s for packed and powder beds.

Further attempts to precise theoretical estimates of the effective thermal conductivity like in Eqs. (1) and (2) (Refs. 12–15) could show excellent coincidence with experiments for certain kinds of heterogeneous media as well as considerable disagreement in other cases. Thus, the three parameters of λ_g, λ_s, and f_s were supposed to be insufficient to describe various heterogeneous media. It became clear that at least a more careful characterizing of the morphology is necessary. Rigorous calculations for regular structures of spherical, cylindrical, and ellipsoidal inclusions are known,[16–20] as well as the results for a nonideal thermal contact with a

matrix[18–20] polydisperse particles[21] and random structures.[22] Nevertheless, these researches do not clarify if the chosen model morphology matches an actual heterogeneous medium. Any heterogeneous structure specified in detail can be calculated using modern numerical methods.[23] However, the experimental determination of the three-dimensional detailed structure itself can be unfeasible because it often requires a complicated tomography analysis, which is restricted in spatial resolution.

General models[10–15] and models with specified geometry[16–22] do not imply such peculiarities of powder beds as a high difference in thermal conductivity between the matrix and the dispersed phase and the contacts between particles. Therefore, special models were developed for the structure of packed beds[7,9,24–30] and lattices of overlapping spheres.[8,31] Some authors were concentrated on the gas filling pores[24–27] while others considered contacts between particles.[7–9,28–31] The effective contact conductivity λ_e of the simple cubic (SC) structure of equal overlapping spheres can be estimated by the Reimann-Weber formula[8]

$$\lambda_e = \lambda_s \left(\frac{1}{x} + \frac{1}{\pi} \ln \frac{2}{x} \right)^{-1}, \tag{3}$$

where x is the relative contact size measured as the ratio of the contact radius to the sphere radius. Numerical calculations of the temperature distribution in an insulated sphere with two small surface contacts[28] gave results for the fcc and bcc lattices of contacting spheres. Heat transfer between a close-packed structure of equal spheres and a wall was calculated.[30] A numerical method for periodic structures was proposed and applied to the fcc lattice of overlapping spheres.[31]

The above models imply the conductive mechanism of heat transfer both in the solid and the gas phases. The thermal conductivity of gas is known to be independent of its pressure.[32] Therefore, these models cannot explain the strong correlation between the effective thermal conductivity and the gas pressure, which is well known from experiments with powder beds.[8,33,34] The common explanation of this correlation is the increase in the mean-free path in the gas with reducing pressure and the related change from the conductive to the transition and the free molecular mechanisms of heat transfer in pores.[33] However, the quantitative theory of this effect does not exist up to now.

A specific kind of heterogeneous media, namely the powder beds, is studied in this paper. The theoretical analysis is based on the two key features of such media: the first, particles of the solid phase can be clearly distinguished, which form point or small surface contacts between them; the second, the thermal conductivity of the solid phase is considerably greater than that of the gas filling pores.

II. MODEL OF DISCRETE THERMAL RESISTANCES

At high ratios of thermal conductivity of the solid phase to that of the gas phase, $\lambda_s/\lambda_g > 700-1000$, heat transfer in the powder bed is controlled by the gas phase as found experimentally.[13] Such a regime is typical for metallic and often for ceramic powders in air. In the vicinity of the contact point, the gap g between two contacting particles is proportional to the distance from the contact point r squared,[26,27] where the factor of proportionality depends on the curvatures of the contacting surfaces. In the conductive regime, heat-flow density q through this gap is inversely proportional to g, so that $q \sim 1/r^2$. Hence, the heat flow is strictly nonuniform in the volume of a pore and its major part passes through thin gaps near the contacts between particles. In case of small surface contacts, a heat flow through the solid phase is superposed, but the total heat flow is still highly nonuniform. The size of the heat-affected zone of a surface contact is of the order of its size, so that the thermal contacts of a particle with its neighbors are independent at the considered conditions. Such medium can be considered as a network of thermal resistances, each of them corresponding to a contact between neighbor particles. The nodes connecting the resistances correspond to the particles.

Thus, the classical theoretical approach based on the interaction of a single particle with the matrix and requiring a correction for mutual influence of particles at their high density is proposed to abandon. Instead, a strong but localized in space interaction is suggested to start with. This model has been developed for calculating the packed beds and the powder beds in Refs. 9, 26, 27, and 29. The principal object of analysis becomes the contact between two neighbor particles. The mutual influence of two neighbor contacts can be taken into account if necessary.[28] Below, the model of discrete thermal resistances is applied to the packed beds of equal spheres. Let the thermal resistance of a contact be Σ.

A. Regular packing of equal spheres

The effective conductivity can be directly calculated for regular lattices. Thus, the conductivity tensor is reduced to a scalar in the systems with cubic symmetry. Therefore, an estimate of the conductivity in a direction of high symmetry is sufficient. For example, if spherical particles of the same diameter D are packed in a SC lattice [see Fig. 1(a)] and the gradient of the homogenized temperature ∇T is directed along axis [100], the heat flow through the corresponding plane (100) can be found as follows. The temperature difference between the centers of spheres of the upper and the lower monolayers is estimated as $\Delta T = \delta |\nabla T|$, where $\delta = D$ is the interplanar spacing. The heat flux of $\Phi = \Delta T/\Sigma$ passes through a contact between the upper and the lower particles. The area $S = D^2$ of plane (100) corresponds to a contact, so that the effective heat flux density is

$$q = \frac{\Phi}{S} = \frac{\delta |\nabla T|}{S\Sigma}. \tag{4}$$

The definition of the effective thermal conductivity λ_e is

$$q = \lambda_e |\nabla T|. \tag{5}$$

Comparison of Eqs. (4) and (5) results

$$\lambda_e = \frac{\delta}{S\Sigma}. \tag{6}$$

Substituting the interplane spacing δ and the area per contact S into Eq. (6) gives that $\lambda_e = 1/(D\Sigma)$ for the SC packing.

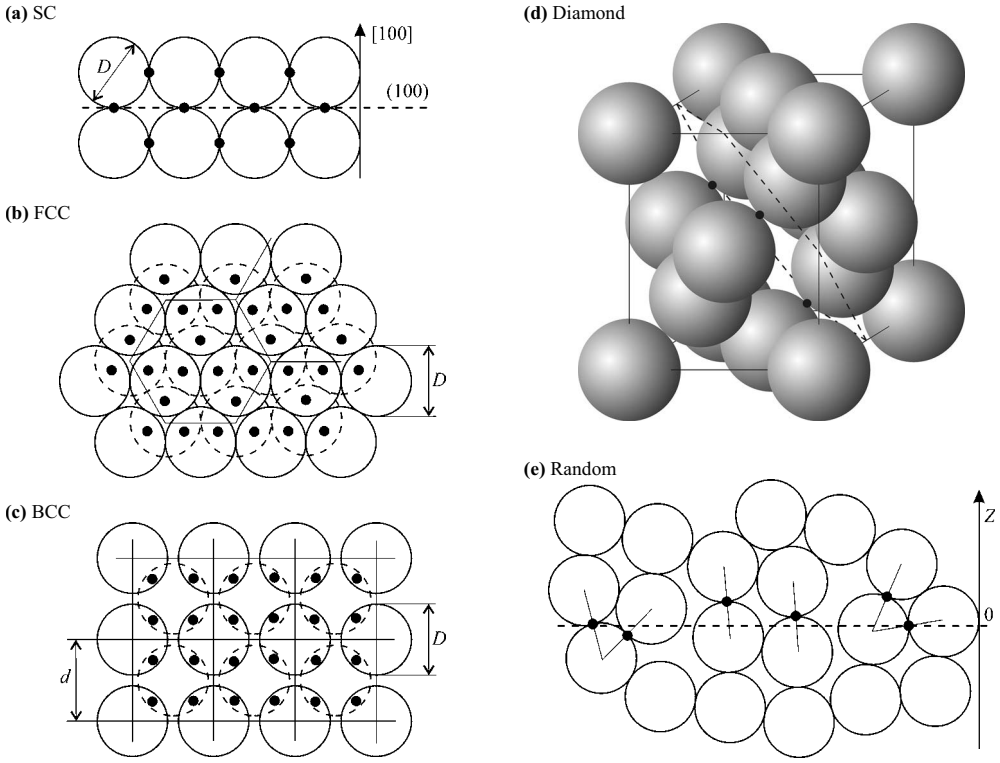

FIG. 1. Thermal contacts (points) at (a)–(d) regular and (e) random packing of equal spheres of diameter D. (a) SC structure. Cross section of two neighbor layers (100): dashed line, plane (100) and arrow, direction [100]. (b) fcc structure. Two neighbor closely packed layers (111): the particles of the lower layer are shown by dashed line and thin lines separate similar hexagons. (c) bcc structure. Two neighbor layers (100): the particles of the lower layer are shown by dashed line, thin lines separate similar squares, and d is the lattice parameter. (d) Diamond structure: thin line, the elementary cube with the side $4(\sqrt{3}/3)D$ and dashed line, plane (111). Only contacts in this plane are shown. (e) Random structure. Axis (OZ) is directed along the vector of temperature gradient. Only contacts contributing to heat transfer through the plane drawn by dashed line are shown. Thin lines connect the centers of contacting particles.

In close-packed structures such as fcc, the effective conductivity in the direction of the normal to the close-packed plane [(111) fcc] can be found as shown in Fig. 1(b). This plane can be divided into regular hexagons shown by thin lines each of them containing nine contacts and has the area of $3(\sqrt{3}/2)D^2$. The average area per contact is $S=(\sqrt{3}/6)D^2$. The interplane spacing is $\delta=(\sqrt{2}/\sqrt{3})D$. These values substituted into Eq. (6) result in the effective thermal conductivity of $\lambda_e=2\sqrt{2}/(D\Sigma)$. In the bcc structure [Fig. 1(c)] with the temperature gradient along axis [100] the interplane spacing equals $\delta=(\sqrt{3}/3)D$. Plane (100) can be divided into squares shown by thin lines with the side equal to the lattice parameter $d=2(\sqrt{3}/3)D$, which contain four contacts. The average area per contact is $S=d^2/4=D^2/3$. Equation (6) with these values of δ and S gives $\lambda_e=\sqrt{3}/(D\Sigma)$. In case of particles packed in the diamond structure with the temperature gradient along axis [111], heat transfer through each regular hexagon in plane (111) shown in Fig. 1(d) is controlled by three contacts. The average area per contact is $S=4(\sqrt{3}/3)D^2$ and the interplane spacing is $\delta=D$, so that $\lambda_e=\sqrt{3}/(4D\Sigma)$. The effective thermal conductivity of the studied regular structures is summarized in Table I.

B. Random packing of equal spheres

The contact between two neighbor particles is characterized by its radius vector $\mathbf{r}$ defined as the middle of the interval connecting the centers of the particles $\mathbf{r}_1$ and $\mathbf{r}_2$, $\mathbf{r}=(\mathbf{r}_1+\mathbf{r}_2)/2$, and the unit vector of direction $\mathbf{\Omega}=(\mathbf{r}_1-\mathbf{r}_2)/|\mathbf{r}_1-\mathbf{r}_2|$. A distribution function of contacts $\varphi(\mathbf{r},\mathbf{\Omega})$ can be introduced with $\varphi d\mathbf{r}d\mathbf{\Omega}$ the number of contacts in elementary volume $d\mathbf{r}$ in solid angle $d\mathbf{\Omega}$. This distribution for a uniform isotropic randomly packed structure of spheres with diameter D is[9]

TABLE I. Parameters of regular structures of equal spheres with cubic symmetry.

Lattice	fcc	bcc	SC	Diamond
Solid fraction, f_s	$\pi\sqrt{2}/6=0.740$	$\pi\sqrt{3}/8=0.680$	$\pi/6=0.524$	$\pi\sqrt{3}/16=0.340$
Coordination number, N	12	8	6	4
Thermal conductivity, $\lambda_e D\Sigma$	$2\sqrt{2}=2.828$	$\sqrt{3}=1.732$	1	$\sqrt{3}/4=0.433$

$$\varphi d\mathbf{r} d\mathbf{\Omega} = \frac{1}{2} f_s N \frac{6 d\mathbf{r}}{\pi D^3} \frac{d\mathbf{\Omega}}{4\pi}, \tag{7}$$

where N is the mean coordination number and the factor of 1/2 in the RHS of Eq. (7) is necessary because two opposite directions $\mathbf{\Omega}$ and $-\mathbf{\Omega}$ correspond to the same contact.

The average heat flux density through plane $z=0$ normal to the vector of temperature gradient ∇T [see Fig. 1(e)] can be found from the distribution function

$$q = \int_{4\pi} d\mathbf{\Omega} \int_{-D\cos\theta/2}^{D\cos\theta/2} \frac{\Delta T(\theta)}{\Sigma} \varphi dz, \tag{8}$$

where θ is the polar angle. The limits of integration over z and the temperature difference through the contact $\Delta T(\theta) = D\cos\theta |\nabla T|$ are evaluated here with the following assumptions: (i) the contact between two particles contributes to heat transfer through a plane only if the centers of the particles are on the opposite sides relative to the plane; (ii) the temperature difference between the centers of neighbor particles depends on their radius vectors $\mathbf{r}_1$ and $\mathbf{r}_2$ as

$$\Delta T = T(\mathbf{r}_1) - T(\mathbf{r}_2) = (\mathbf{r}_1 - \mathbf{r}_2) \nabla T = D\mathbf{\Omega} \nabla T. \tag{9}$$

The effective thermal conductivity of the random structure is obtained by comparison of definition (5) with the result of integration of Eq. (8)

$$\lambda_e D\Sigma = \frac{f_s N}{\pi}. \tag{10}$$

This equation obtained for statistically isotropic random packing appears to be rigorous for the above considered regular structures too. This can be proved by substituting the parameters from Table I into Eq. (10).

III. THERMAL RESISTANCE OF A CONTACT BETWEEN TWO PARTICLES

To evaluate the resistance Σ, heat transfer between two contacting spheres of radii R_1 and R_2 is considered as shown in Fig. 2. The temperatures of the centers of the spheres are T_1 and T_2. The gap between the spheres is filled with a gas of thermal conductivity λ_g, which is much less than those inside the spheres λ_1 and λ_2. A small circular surface contact of radius a much less than R_1 and R_2 is possible between the spheres (see Fig. 2). In the considered conditions, the principal part of the heat flux is transferred through the vicinity of the contact where the gap g between the spheres is approximated by a quadratic function of distance r from the center of the contact (see Fig. 2)

$$g = \frac{r^2}{R}, \tag{11}$$

with the reduced radius

$$R = \frac{2R_1R_2}{R_1 + R_2}. \tag{12}$$

The steady-state temperature distribution in the solid phase satisfies the equation of Laplace

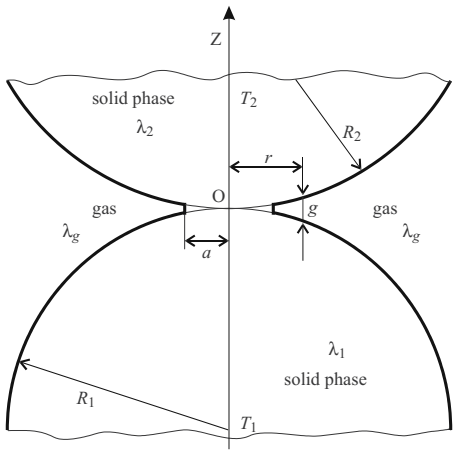

FIG. 2. Thermal contact between two spheres of radii R_1 and R_2, thermal conductivities λ_1 and λ_2, and temperatures in their centers T_1 and T_2. a is the radius of the surface contact, r is the distance from the axis of symmetry (OZ), g is the gas gap, and λ_g is the thermal conductivity of gas.

$$\frac{\partial^2 T}{\partial z^2} + \frac{1}{r}\frac{\partial}{\partial r}\left(r\frac{\partial T}{\partial r}\right) = 0, \tag{13}$$

where the cylindrical system of coordinates (z,r) is introduced with axis (OZ) connecting the centers of the particles and point $(z=0,\ r=0)$ corresponds to the center of the contact (see Fig. 2). Equation (11) suggests that $g \ll r \ll R$ in the studied domain near the contact. Therefore, the gap g can be neglected when specifying the boundary conditions at the spheres. The approach where solid phase one occupies the bottom half space $z<0$ and solid phase two occupies the upper half space $z>0$ is applied below. The condition of continuity of heat flow q between the particles is written as

$$\lambda_1 \left.\frac{\partial T}{\partial z}\right|_{z=-0} = \lambda_2 \left.\frac{\partial T}{\partial z}\right|_{z=+0} = q(r). \tag{14}$$

The other boundary conditions are the temperature continuity at the surface contact

$$T|_{z=-0} = T|_{z=+0} \quad \text{at} \quad r < a \tag{15}$$

and the condition of temperature jump on the gas gap

$$h(T|_{z=+0} - T|_{z=-0}) = q(r) \quad \text{at} \quad r < a, \tag{16}$$

where h is the heat transfer coefficient through the gas gap $g(r)$. The centers of the spheres are far from the heat-affected zone of the contact, so that in the considered approximate geometry one can specify temperatures T_1 and T_2 at the infinity

$$T \to T_1 \quad \text{at} \quad z \to -\infty, \tag{17}$$

$$T \to T_2 \quad \text{at} \quad z \to -\infty. \tag{18}$$

Thus, the problem of thermal contact between spheres is approximated by the problem of nonideal thermal contact between half spaces. The temperature distribution in half spaces $z<0$ and $z>0$ is found from the equation of Laplace (13) with boundary conditions on the contact surface [Eqs.

(14)–(16)] and conditions at the infinity [Eqs. (17) and (18)]. The precision of this approximation increases when the size of the heat-affected zone decreases relative to the sizes of the spheres, i.e., when the radius of the surface contact a decreases relative to R (see Ref. 9) and the gas conductivity λ_g decreases relative to conductivities of solid phases λ_1 and λ_2.[26,27] After introducing dimensionless temperature

$$\tau = \begin{cases} (T - T_c)/(T_c - T_1), & z < 0 \\ (T - T_c)/(T_2 - T_c), & z > 0 \end{cases}, \tag{19}$$

where $T_c = (\lambda_1 T_1 + \lambda_2 T_2)/(\lambda_1 + \lambda_2)$ is the temperature of the surface contact, boundary problem [Eqs. (13)–(18)] becomes antisymmetric relative to plane $z=0$, namely, $\tau(-z,r) = -\tau(z,r)$, and is reduced to a half-space problem. For example, in half space $z>0$

$$\frac{\partial^2 \tau}{\partial z^2} + \frac{1}{r}\frac{\partial}{\partial r}\left(r\frac{\partial \tau}{\partial r}\right) = 0, \tag{20}$$

$$\tau|_{z=0} = 0 \quad \text{at} \quad r < a, \tag{21}$$

$$\tau|_{z=0} = \frac{\lambda_s}{2h} \left.\frac{\partial \tau}{\partial z}\right|_{z=0} \quad \text{at} \quad r > a, \tag{22}$$

$$\tau \to 1 \quad \text{at} \quad z \to \infty \tag{23}$$

where

$$\lambda_s = \frac{2\lambda_1 \lambda_2}{\lambda_1 + \lambda_2} \tag{24}$$

is the reduced conductivity of the solid. The heat flux density through the contact is evaluated as

$$q(r) = \frac{\lambda_s}{2}(T_2 - T_1) \left.\frac{\partial \tau}{\partial z}\right|_{z=0}. \tag{25}$$

The thermal resistance Σ can be found from the following equation

$$\frac{1}{\Sigma} = \frac{1}{T_2 - T_1}\int_0^\infty q(r) 2\pi r dr = \pi \lambda_s \int_0^\infty \left.\frac{\partial \tau}{\partial z}\right|_{z=0} r dr. \tag{26}$$

A. Heat transfer through the gas gap

The heat transfer coefficient h through the gas gap g should be defined to fully specify the considered problem. In the conductive limit it equals

$$h = \frac{\lambda_g}{g}. \tag{27}$$

When the gap reduces, Eq. (27) is disturbed by nonequilibrium boundary layers with the thicknesses of the order of the mean-free path.[32] This can be taken into account by introducing the interfacial thermal resistance. For a thin gap comparable with the mean-free path in the gas, heat transfer is calculated from the Boltzmann equation. A good approximation can be the well-known problem of heat transfer between parallel plates for the Boltzmann equation[32] because the spherical surfaces are approximately parallel near the contact. Points in Fig. 3 show numerical results obtained by 12-moment approximation for gas with internal degrees of freedom.[35] These data comprise the effect of the interfacial thermal resistance taken into account through the gas kinetic boundary conditions.[35] In these calculations, gap g is normalized by the mean-free path l, which is related with the dynamic viscosity μ. Thus, for the Maxwell molecules[32]

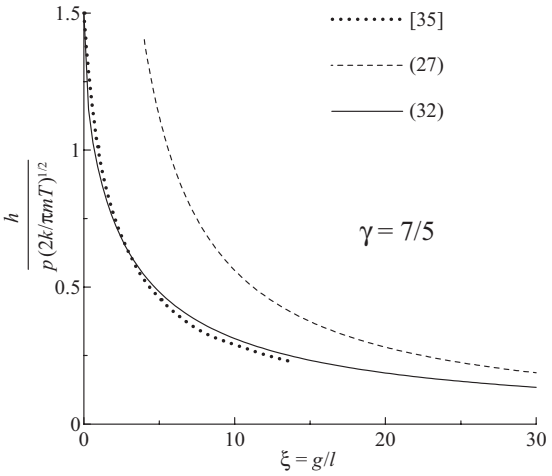

FIG. 3. Heat transfer coefficient h between parallel plates at distance g in gas with the mean-free path l at $\gamma=7/5$; dotted line, numerical calculation in 12-moment approximation (Ref. 35); dashed line, conductive limit at $\xi \gg 1$ (27); and full line, approximation by Eq. (32).

$$\mu = \frac{\sqrt{\pi}}{3} mnl\bar{v}, \tag{28}$$

where $n=p/kT$ is the molecular density of the gas, m is the molecular mass, p is the pressure, k is the Boltzmann constant, and $\bar{v} = (8kT/\pi m)^{1/2}$ is the mean molecular velocity. Thermal conductivity λ_g and viscosity μ of gas are approximately related by the Eucken equation[32]

$$\lambda_g = \frac{1}{4}(9\gamma - 5) c_v \frac{\mu}{m}, \tag{29}$$

where γ is the adiabatic exponent and $c_v = k/(\gamma - 1)$ is the specific heat at constant volume. The following definition of the mean-free path through the thermal conductivity λ_g can be obtained from Eqs. (28) and (29)

$$l = 6\frac{\gamma - 1}{9\gamma - 5}\frac{\lambda_g}{p}\left(\frac{mT}{2k}\right)^{1/2}. \tag{30}$$

The heat transfer coefficient h tends to its free molecular limit[35]

$$h_0 = \frac{1}{4}\frac{\gamma + 1}{\gamma - 1} p \left(\frac{2k}{\pi mT}\right)^{1/2}, \tag{31}$$

at $\xi = g/l \ll 1$ and to the conductive limit (27) shown in Fig. 3 at $\xi \gg 1$. In the present paper the following approximation for the function $h(\xi)$ is used

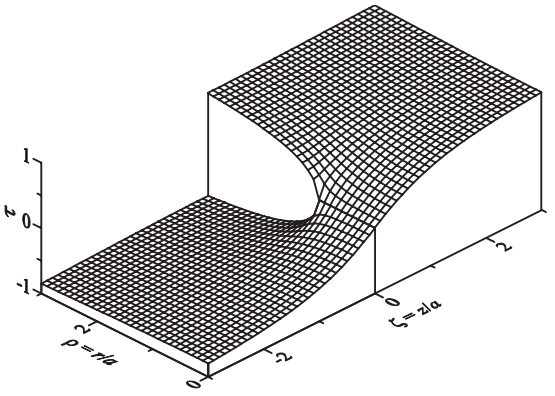

FIG. 4. Distribution of the dimensionless temperature $\tau(z,r)$ in the heat-affected zone of a circular contact with radius a between two insulated half spaces with different temperatures.

$$\frac{h}{h_0} = \frac{1}{2}\frac{1}{1+\xi/\chi} + \frac{1}{2}\frac{1}{[1+(\xi/\chi)^{1/2}]^2}, \quad \chi = \frac{2\sqrt{\pi}}{3}\frac{9\gamma-5}{\gamma+1}, \tag{32}$$

which is shown by full line in Fig. 3. Equation (32) exactly tends to the free molecular and conductive limits and correctly approximates results[35] for the transition regime (see Fig. 3).

B. Limit of low thermal conductivity of gas

The studied problem reduces to that of circular contact between two ideally insulated half spaces if the heat flux though the gas gap can be neglected. When $h \to 0$ in Eq. (22), it becomes the adiabatic condition

$$\left.\frac{\partial \tau}{\partial z}\right|_{z=0} = 0 \quad \text{at} \quad r > a. \tag{33}$$

The rigorous analytic temperature distribution in the solid phase is known at this condition[9]

$$\tau = 1 - \frac{2}{\pi}\text{arctg}\frac{\sqrt{2}}{\sqrt{\rho^2+\zeta^2-1+\sqrt{(\rho^2+\zeta^2-1)^2+4\zeta^2}}} \text{at} \quad \zeta > 0, \tag{34}$$

with dimensionless coordinates $\rho = r/a$ and $\zeta = z/a$. This distribution shown in Fig. 4 is discontinuous on the insulating wall $\{z=0,\ r>a\}$. The temperature gradient attains the maximum at the contact. The temperature tends to the constant values at the distance of several contact diameters from its center, which shows that the heat-affected zone is localized and the model of discrete thermal resistances can be applied. The contact resistance is evaluated by substituting Eq. (34) into Eq. (26)

$$\Sigma = \frac{1}{2\lambda_s a}. \tag{35}$$

This result corresponds to the well-known problem of a circular heat source with a constant temperature on an insulated half space.[36] The effective thermal conductivity of the packed bed of equal spheres is obtained by substituting Eq. (35) into Eq. (10)

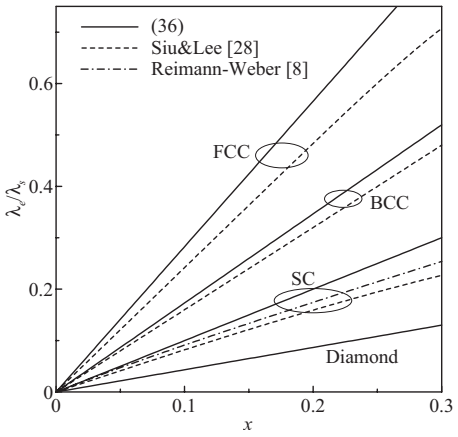

FIG. 5. Effective thermal conductivity λ_e normalized by the conductivity of solid λ_s versus the relative contact size x. Comparison of the present model [Eq. (36), full lines] with the models by Siu and Li (Ref. 28, dashed lines) and Reimann-Weber [Ref. 8, Eq. (3), dash-dotted line] for equal spheres packed in cubic lattices.

$$\frac{\lambda_e}{\lambda_s} = \frac{f_s N}{\pi} x, \tag{36}$$

where $x = a/R = 2a/D$ is the relative contact size. This equation is valid for the regular lattices with parameters f_s and N listed in Table I as well as for the random structure. The effective conductivity is proportional to the contact size with the factor of proportionality strongly depending on the structure through the volume fraction of solid f_s and the coordination number N. Figure 5 shows that the model of Reimann-Weber (3) and the numerical calculations of Siu and Li,[28] give slightly nonlinear dependencies of the conductivity versus the contact size x. This nonlinearity can be considered as the consequence of the mutual influence of neighbor contacts. When x tends to zero, the heat-affected zones of contacts decrease, the interaction vanishes, and the Reimann-Weber (3) gives exactly the same result as Eq. (36) with the parameters of the SC lattice. The present model somewhat overestimates the effective conductivity at greater values of x. It is in satisfactory agreement with the known models at least in the interval $0 < x < 0.3$ as shown in Fig. 5.

The above analysis indicates that the effective thermal conductivity of packed (powder) beds with surface contacts between particles essentially depends on three structure parameters: the volume fraction of solid f_s, the coordination number N, and the relative contact size x. Nevertheless, the only discussed parameter was f_s in numerous experimental studies of the thermal conductivity of slightly sintered powders stimulated by the development of the technology of selective laser sintering.[37–39] A correlation between N and f_s is probable. An example of such a correlation is given by the regular structures in Table I. However, different coordination numbers are possible at the same porosity in real random structures, so that the two parameters are better considered independently.

C. Low thermal conductivity of gas at point contacts between particles

If the particles do not form surface contacts, the flux transferred through the solid phase equals zero. Therefore the flux transferred through the gas gap cannot be neglected even at low thermal conductivity of gas. When the conductivity of gas decreases relative to the conductivity of solid, the heat transfer is controlled by the gas and the temperature distribution in the particles approaches to the uniform one. At the limit of low conductivity of gas, the temperatures of particle surfaces equal to their temperatures at the centers and Eqs. (16) and (26) result in

$$\frac{1}{\Sigma} = \int_0^\infty h(r) 2\pi r dr, \tag{37}$$

where the heat transfer coefficient h is specified by Eq. (32) as the function of the gap g. The quadratic function $g(r)$ given by Eq. (11) cannot be used because it produces a logarithmic divergence at $r \to \infty$. The upper integration limit in Eq. (37) was suggested to cut at $r \sim R$,[26,27] when the approximation by Eq. (11) becomes incorrect. A high precision of the estimate of this limit is not required because of the logarithmic dependence on it. The physical reason of such a cutting is that the gap between two spheres is defined at r less than the radii of the spheres.

The value of the cutting radius was obtained in Refs. 26 and 27 by partitioning the sphere area between N nearest neighbors. This approach gives a slow dependence of the result on the coordination number. In this paper, the contact resistance and the packing structure are analyzed separately, so that a simplified cutting method is used

$$\frac{1}{\Sigma} = \int_0^R h(r) 2\pi r dr, \tag{38}$$

which results in the thermal resistance of contact Σ independent of N

$$\lambda_g D\Sigma = \frac{2}{\pi} \frac{1}{\frac{1}{2}\ln(1+L) + \ln(1+\sqrt{L}) + \frac{1}{1+\sqrt{L}} - 1}, \tag{39}$$

where

$$L = \frac{\gamma+1}{9\gamma-5} \frac{3}{4\sqrt{\pi} Kn} \tag{40}$$

and $Kn = l/D$ is the Knudsen number.

Equations (10) and (39) result in the explicit formula for the effective thermal conductivity of the packed bed of equal spheres

$$\frac{\lambda_e}{\lambda_g} = \frac{f_s N}{2} \left[\frac{1}{2}\ln(1+L) + \ln(1+\sqrt{L}) + \frac{1}{1+\sqrt{L}} - 1 \right], \tag{41}$$

where the expression in square brackets depends on the gas parameters and the factor before it is the dependence on the packing parameters f_s and N, which is the same as in Eq. (36). The effective conductivity (41) is related with the particle size and the gas pressure through the Knudsen number.

D. Numerical calculation

Boundary problem [Eqs. (21)–(23)] for the equation of Laplace (20) in a half space is numerically solved by a finite-volume method of the second order. First Eq. (20) is solved in finite domain $\{0 < z < Z_m,\ 0 < r < R_m\}$ with condition $\tau = 1$ at boundaries $z = Z_m$ and $r = R_m$. Then Z_m and R_m are increased step by step to find the limit at $Z_m \to \infty$ and $R_m \to \infty$. The computation grid is uniform both in z and r. The gap between two spheres necessary to evaluate the heat transfer coefficient (32) is found as

$$g = \begin{cases} 2(R - \sqrt{R^2 - r^2}), & r \le R \\ \infty, & r > R \end{cases}. \tag{42}$$

The contact resistance Σ is calculated by numerical integration of Eq. (26).

Examples of the obtained distributions of the heat flow and the surface temperature of the particle versus the distance r from the center of the contact are shown in Fig. 6. These calculations are made on the grid 800×800, where first 20 cells in r can be projected inside the surface contact $r < a$. When the conductivity ratio λ_s/λ_g increases, these distributions tend to the limits shown by dashed lines, which follow from the model of circular contact between two insulated half spaces (34)

$$\tau|_{\zeta=0} = \begin{cases} 0 & \rho < 1 \\ 1 - \frac{2}{\pi} \mathrm{arctg} \frac{1}{\sqrt{\rho^2 - 1}}, & \rho > 1 \end{cases}, \tag{43}$$

$$\frac{2aq}{\lambda_s (T_2 - T_1)} = \left. \frac{\partial \tau}{\partial \zeta} \right|_{\zeta=0} = \begin{cases} \frac{2}{\pi\sqrt{1-\rho^2}} & \rho < 1 \\ 0 & \rho > 1 \end{cases}. \tag{44}$$

The heat flux density q (left column in Fig. 6) transferred through the gas phase at $r > a$ is considerably less than in the solid phase at $r < a$ and sharply decreases with r. This justifies the model of discrete resistances. The temperature shown in the right column of Fig. 6 approaches to a constant value with increasing r. If the Knudsen number Kn decreases, the mentioned distributions in gas (dotted lines in Fig. 6) tend to the conductive limit $Kn = 0$ (full lines). Approaching to the limit is slower at smaller relative contact size $x = a/R$. Thus, Fig. 6(c) shows a significant difference in the heat flux at $Kn = 10^{-4}$ and $Kn = 0$. This is because the Knudsen number is defined by the particle diameter D but the heat flux is controlled by the gas gap g, which can be much smaller than D.

The dimensional analysis of problem [Eqs. (20)–(23) and (32)] and the comparison with limiting cases [Eqs. (35) and (39)] indicate that the contact resistance generally depends on four dimensionless parameters

$$\lambda_g D\Sigma = F\left(x, \frac{\lambda_s}{\lambda_g}, Kn, \gamma\right), \tag{45}$$

where $F(\,)$ is a dimensionless function. In the conductive limit $Kn = 0$, when the dependence on the last two parameters vanishes, the calculated contact resistance Σ is shown in Fig. 7 versus x and λ_s/λ_g. The normalization of Σ is changed in

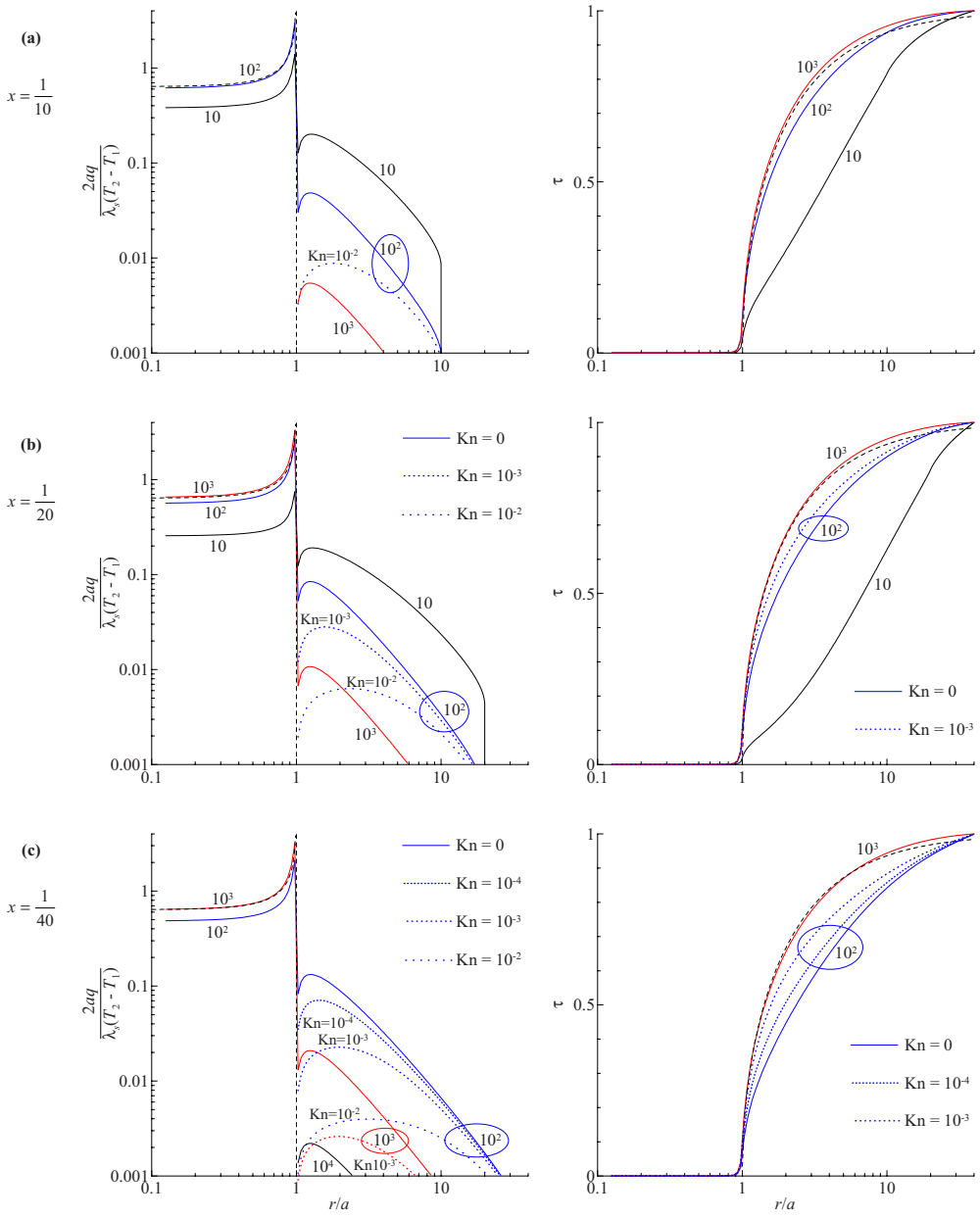

FIG. 6. (Color online) Normalized heat flux density q (left column) through the contact between two spherical particles with center temperatures T_1 and T_2 and the dimensionless temperature τ (right column) on the particle surface versus the distance r from the center of contact. The ratio of the radius of the surface contact to the reduced radius of the particles $x=a/R$: (a) 1/10; (b) 1/20; and (c) 1/40. Full lines show the conductive limit $Kn=0$ with the numbers near the curves indicating the ratio λ_s/λ_g of the reduced conductivity of solid to the conductivity of gas. Dashed lines show the limit at $\lambda_g=0$. Dotted lines show the transition regime in the gas with the adiabatic exponent $\gamma=7/5$ and indicated values of the Knudsen number Kn.

this figure to facilitate the comparison with the model of circular contact between insulated half spaces (35). Figure 7 shows that in the shadowed domain of parameters, this limiting model can be applied with the relative error less than 10%. Decreasing the resistance with decreasing x and λ_s/λ_g means increasing the relative input of heat transfer through the gas gap between particles. Figure 8 shows the influence of rarefying the gas, where full lines are the sections of the surface shown in Fig. 7 at constant x and points are calculations at nonzero Kn. As Kn increases, the contact resistance increases because of decreasing the flux through the gas gap (compare with Fig. 6) and approaches to the model of circular contact between insulated half spaces (35).

Figure 9 shows the examples of calculation at $x=0$ when the particles form point contacts but not surface ones. In this case, a grid 100×100 in the calculation domain with the dimensions $R_m=Z_m=R$ was sufficient. The heat flux density q [Fig. 9(a)] steeply decreases with the distance from the contact center and the surface temperature of the particle can be strongly nonuniform, for example at $Kn=10^{-4}$ and $\lambda_s/\lambda_g=10$ and 10^2 in Fig. 9(b), as well as approximately constant, for example at $Kn=10^{-4}$ and $\lambda_s/\lambda_g=10^3$ and 10^4. Heat transfer is controlled by gas phase in the latter case. The dependence on the adiabatic exponent γ is very slow in these

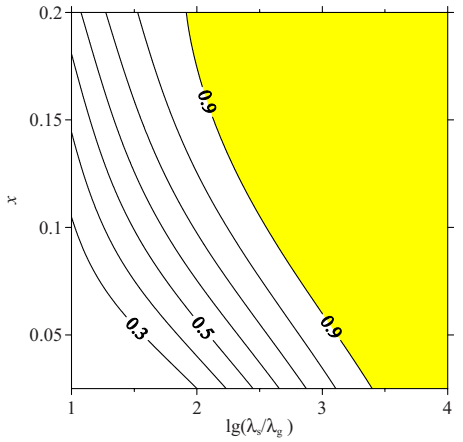

FIG. 7. (Color online) Dimensionless thermal resistance of a contact between two spheres $2a\lambda_s\Sigma$ in the conductive limit $Kn=0$ versus the relative size of the surface contact $x=a/R$ and the conductivity ratio λ_s/λ_g. In the shadowed domain [Eq. (35)] for the circular contact between half spaces provides a good approximation.

examples. Figure 10 shows the sections of the surface of dimensionless contact resistance (45) in the parameter space at $x=0$ and constant Kn and γ. These sections appear to depend on γ very weakly. When the conductivity ratio λ_s/λ_g increases, the relative contribution of the gas phase into the contact resistance increases and the resistance tends to the limit equal to the resistance of the gas gap, which depends on the Knudsen number and is estimated by Eq. (39) (horizontal intervals in Fig. 10). When the Knudsen number decreases, the distance between the corresponding curves decreases in the left bottom part of Fig. 10, especially at $\lambda_s/\lambda_g<10^2$ and $Kn<10^{-4}$, indicating the tendency to the conductive limit at $Kn=0$ shown by the dotted line.

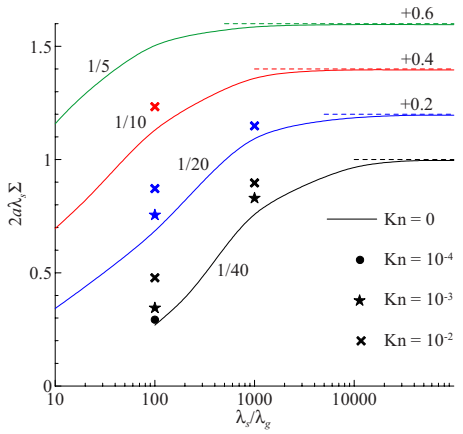

FIG. 8. (Color online) Dimensionless contact thermal resistance $2a\lambda_s\Sigma$ versus the conductivity ratio λ_s/λ_g at the relative size of the surface contact $x=a/R$: 1/40; 1/20; 1/10; and 1/5. The values of x are indicated near curves. Full lines show the conductive limit $Kn=0$. The curves are vertically shifted with the increment of 0.2 and the indicated absolute shift. Dashed horizontal lines show the limit at $\lambda_g\to 0$. Points show the transition regime in gas with the adiabatic exponent $\gamma=7/5$ and the indicated values of the Knudsen number Kn.

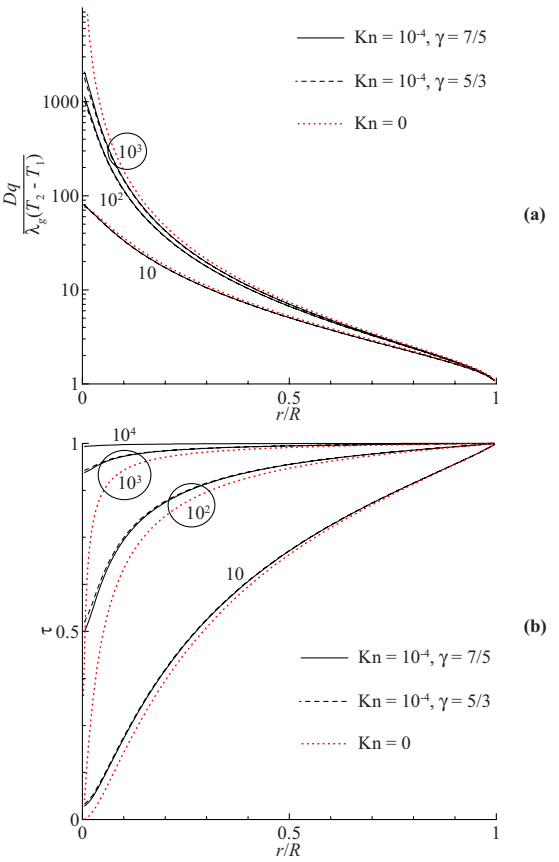

FIG. 9. (Color online) Normalized heat flux density q (a) through the gas gap between two spherical particles in a point contact with the temperatures of their centers T_1 and T_2 and the dimensionless temperature τ (b) on the particle surface versus the distance r from the contact point at $Kn=10^{-4}$ and $\gamma=7/5$ (full lines) and $\gamma=5/3$ (dashed lines) and in the conductive limit $Kn=0$ (dotted lines). The numbers near the curves indicate the ratio λ_s/λ_g of the reduced thermal conductivity of the solid phase to the thermal conductivity of the gas.

In the case of the point contact, the gas gap g between particles can be arbitraryly small when approaching to the contact point and the zones of molecular heat transfer in gas where $g\ll l$ and the transition heat transfer with $g\sim l$ always exist. When the Knudsen number decreases, the curves approach each other in the left bottom of Fig. 10 at $\lambda_s/\lambda_g<10^2$ and slowly tend to the conductive limit $Kn=0$ shown by dashed line. The conductive approximation (27) considerably overestimates the heat transfer coefficient in these zones. Nevertheless, the estimates implementing Eq. (27) instead of a more rigorous Eq. (32) shown in Figs. 9 and 10 by dotted lines are useful and do tend to a finite limit at $Kn\to 0$. This is because at low Kn near the contact point where approximation (27) could introduce a considerable error, the heat transfer is controlled by the solid phase.

IV. ANALYSIS OF EXPERIMENTAL DATA

The effective thermal conductivity of powder and packed beds is evaluated by the model of discrete thermal resis-

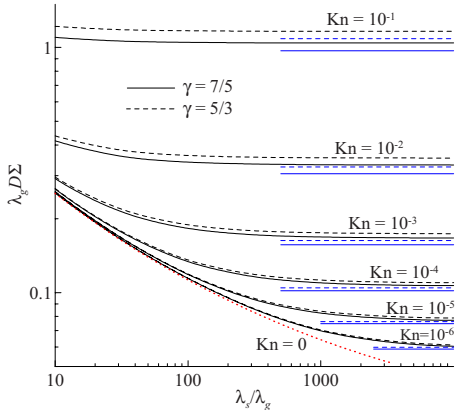

FIG. 10. (Color online) Dimensionless thermal resistance $\lambda_g D\Sigma$ versus the conductivity ratio λ_s/λ_g at the point contact $x=0$. The values of the Knudsen number Kn are indicated near the corresponding curves. The adiabatic exponent γ: 7/5 (full lines) and 5/3 (dashed lines) are given. The dotted line shows the conductive limit $Kn=0$. Horizontal intervals show the limit at $\lambda_g \to 0$.

tances (10) where the results of Sec. III are useful to estimate the contact resistance between two particles Σ. The necessary gas parameters are listed in Table II. The thermal conductivity of gases is taken from Ref. 40 and the mean-free path at the normal pressure is calculated by Eq. (30).

The method of calculation is explained below by the example of packed bed of glass spheres with diameter $D=4.06$ mm in air at the temperature of 60 °C and the atmospheric pressure studied in Ref. 24. Table III presents the parameters for calculation and the results. The parameters of air are taken from Table II at the temperature of 333 K. According to Fig. 10, the dimensionless parameters of the contact are near the limiting curve at $Kn \to 0$. The numerical model described in Sec. III results in the dimensionless contact resistance $\lambda_g D\Sigma=0.141$. Equation (10) for the effective thermal conductivity requires the mean coordination number N, which was not measured in Eq. (24). However, the reported value of the solid fraction $f_s=0.6$ is intermediate between bcc and SC structures (see Table I), so that the value of N is supposed to be intermediate. The estimate of $N=7$ gives $\lambda_e/\lambda_g=9.5$, while the experimental value of λ_e/λ_g reported in Eq. (24) equals 12.0.

TABLE II. Parameters of gases at the atmospheric pressure accepted for calculation.

Gas	Temperature, T (K)	Adiabatic exponent, γ	Thermal conductivity, λ_g [W/(m K)]	Mean-free path, l (nm)
Air	298	7/5	0.026	58
Air	333	7/5	0.029	69
N_2	298	7/5	0.0257	57
He	298	5/3	0.152	161
He	473	5/3	0.2	266
He	573	5/3	0.24	352
Ar	298	5/3	0.0177	59

The discrepancy can arise because of neglecting the radiative heat transfer in the calculations. The radiative contribution to the thermal conductivity is estimated in the Rosseland approximation as[41]

$$\lambda_r = \frac{16\sigma T^3}{3\beta}, \tag{46}$$

where β is the effective extinction coefficient for the thermal radiation and σ is the constant of Stefan-Boltzmann. The wavelength of the thermal radiation is about 10 μm at the considered temperature. The glass is opaque at this wavelength. In the heterogeneous medium composed of opaque and a transparent phases, the effective extinction coefficient is estimated as a quarter of the specific surface of the interface per the unit volume of the transparent phase.[42] In the case of the packed bed of spheres, this gives

TABLE III. Calculation of the packed bed of glass spheres in air at 60 °C and the atmospheric pressure.

Parameter	Value	Source, note
Sphere diameter, D	4.06 mm	Ref. 24 Initial data
Volume fraction of the solid phase, f_s	0.60	Ref. 24
Thermal conductivity of the solid, λ_s	1.61 W/(m K)	Ref. 24
Relative size of the surface contact, $x=2a/D$	0	Dimensionless parameters for evaluating the contact resistance by Eq. (45)
Conductivity ratio λ_s/λ_g	56	
Knudsen number, $Kn=l/D$	$1.70\cdot10^{-5}$	
Adiabatic exponent, γ	7/5	
Dimensionless contact resistance, $\lambda_g D\Sigma$	0.141	Numerical calculation, Fig. 10
Mean coordination number, N	7	Estimate by Table I
Dimensionless effective thermal conductivity, λ_e/λ_g	9.5	Calculation by Eq. (10)
	10.2	With the correction for radiative thermal conductivity by Eq. (48)
	11.0	Evaluation by empirical formula, Ref. 24
	12.0	Experimental value, Ref. 24

$$\beta = \frac{f_s}{1-f_s}\frac{3}{2D}. \quad (47)$$

Substitution of Eq. (47) into Eq. (46) gives the estimate of the radiative thermal conductivity

$$\lambda_r = \frac{32}{9}\frac{1-f_s}{f_s} D\sigma T^3, \quad (48)$$

which results in $\lambda_r = 0.020$ W/(m K) $= 0.7\lambda_g$. The contact and radiative heat flows are approximately independent, so that the corresponding conductivities should be added. Thus, the calculated value with the correction for the radiative transfer is about $10.2\lambda_g$, which is still less than the experimental value of $12\lambda_g$. The estimation by the empirical formula[24] gives $\lambda_e/\lambda_g = 11.0$, which underestimates the experiment too. The difference between the calculated and the experimental values can be explained by the formation of small surface contacts between particles due to a surface contamination or a deformation.

A. Dependence on the gas pressure

Numerical calculation by the model results in S-shaped curves of the effective thermal conductivity λ_e of the packed bed versus the pressure p of the gas filling pores, which are shown by full lines in Fig. 11. The right branches of these curves tend to the limit of $Kn=0$ (dashed line in Fig. 11(a) at $p \to \infty$, which corresponds to the dotted curve in Fig. 10. In the considered case of point contacts between particles, $x=0$, the left branches tend to zero.

Experimental works often report the residual thermal conductivity at zero pressure. This value was $0.42\lambda_g$ for experiment[25] shown by points in Fig. 11(a). The residual conductivity is the sum of the conductivity through the surface contacts (at $x>0$) given by Eq. (36) and the radiative conductivity given by Eq. (48). The contribution of the radiative conductivity is evaluated as about $0.12\lambda_g$ in the considered conditions. Then the rest of $0.3\lambda_g$ can be used to estimate the relative size of the surface contact by Eq. (36). This results in $x = 3 \cdot 10^{-3}$. Such a small value can be explained by a noncontrolled contamination.

The calculated curves (full lines in Fig. 11) are generally in good agreement with experiments[25,33] for the packed beds of ceramic particles (points). However, the experimental values tend to the right limit a bit faster than the calculated ones. According to the model, the value of the right limit is sensible to the ratio λ_s/λ_g. While the conductivity of gas λ_g is known with a good accuracy (see Table II), the conductivity of solid ceramic phase λ_s could be a source of error. In the calculations the values for pure sintered oxides[40] are used, which are indicated on the left top corner of each diagram. These values could considerably overestimate the actual conductivity of the solid phase because of impurities and crystal defects probably present in small particles. If the ratio λ_s/λ_g were less, the saturation of the contact resistance with decreasing the Knudsen number Kn (see Fig. 10) would occur earlier. The gas pressure is inversely proportional to Kn (see upper horizontal axes in Fig. 11), so that the corresponding saturation with increasing the pressure would occur earlier and the limit value would be less.

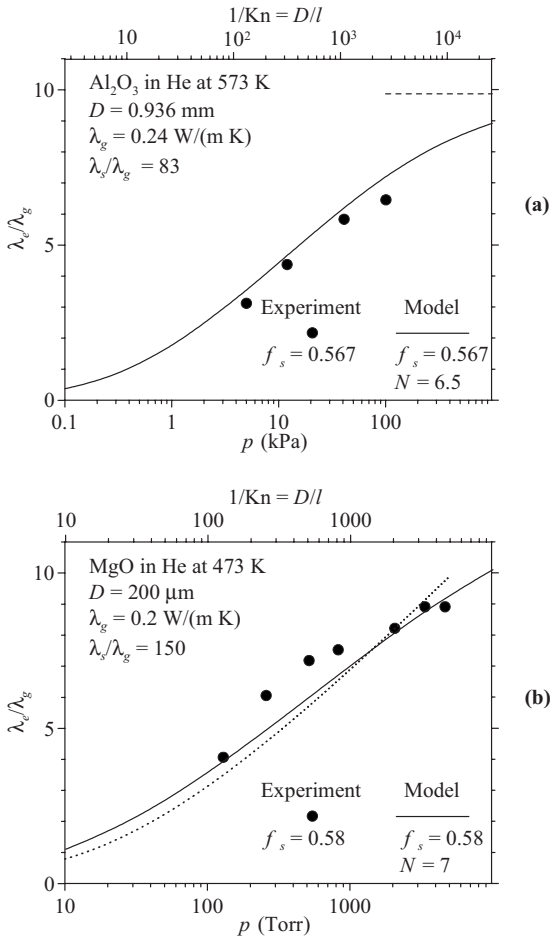

FIG. 11. Effective thermal conductivity λ_e of packed beds of ceramic particles in He versus pressure p: (a) spheroids Al_2O_3 with the diameter $D=0.936$ mm at the temperature 573 K (Ref. 25) and (b) powder Al_2O_3 with the mean diameter of particles $D=200$ μm at the temperature 473 K (Ref. 33). Points show experimental data of Refs. 25 and 33. Full lines show the numerical calculations. The horizontal dashed line shows the limit at $Kn=0$. The dotted line shows the approximation of isothermal spheres (41).

The left and the central parts of the S curve can be independent of the conductivity of the solid phase because the contact resistance approaches to its limit at $\lambda_s/\lambda_g \to \infty$ (see Fig. 10) as Kn increases. In this limit the contact resistance is estimated by the model of isothermal spheres (horizontal intervals in Fig. 10) where the effective thermal conductivity is given by Eq. (41). The dotted curve in Fig. 11(b) calculated by this approach satisfactorily agrees with the shown experimental data.

The approximation of isothermal spheres (41) becomes more precise with increasing the ratio λ_s/λ_g, so that it is useful for metallic particles of high thermal conductivity. Figure 12 compares this approximation with experimental data[34] for packed beds of uranium spheres. Thermal conductivity of uranium at RT is about $\lambda_s = 28$ W/(m K),[40] which results in the ratio of about $\lambda_s/\lambda_g = 1000$ in nitrogen atmosphere (see the value of λ_g in Table II). According to Fig. 10, at such a high ratio λ_s/λ_g the approximation of isothermal spheres should be satisfactory at $Kn > 10^{-4} \div 10^{-5}$, which cor-

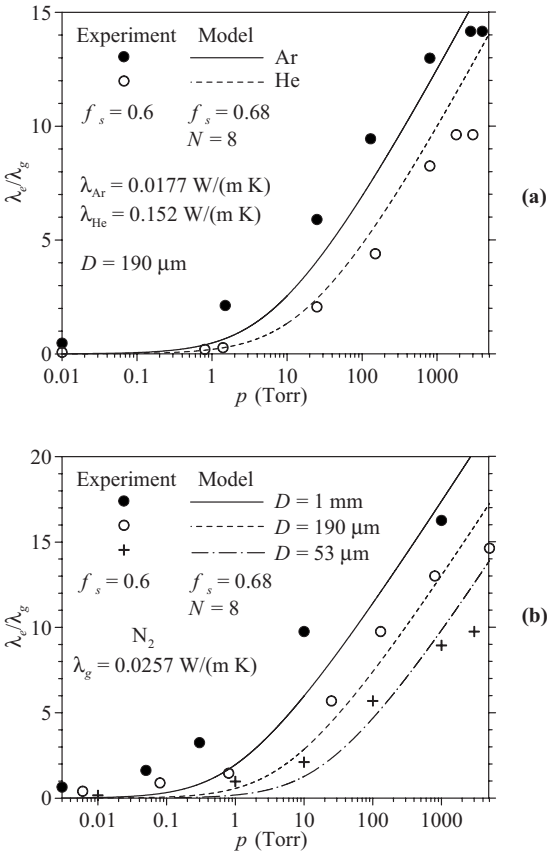

FIG. 12. Comparison of the function of the effective thermal conductivity λ_e versus the pressure p calculated in the approximation of isothermal spheres (41) (curves) with the experimental data of Ref. 34 (points) for packed beds of uranium spherical particles in gases at the RT: (a) particles of diameter $D=190$ μm in Ar and He and (b) particles of various diameters in N_2.

responds to the particle diameter $D<0,6\div6$ mm at the atmospheric pressure in nitrogen with $l=57$ nm. Indeed, the calculations by this simplified model agree with the experimental data in Fig. 12.

B. Dependence on the nature of gas

At the same structure parameters f_s and N and the adiabatic exponent γ Eq. (41) specifies the dimensionless ratio λ_e/λ_g as a universal function of the Knudsen number. Therefore, changing a monatomic gas to another monatomic gas in the same packed bed is equivalent to shifting the universal curve along the axis of pressure according to the change in the mean-free path. This is demonstrated by Fig. 12(a). The helium atom is smaller than that of argon. Therefore, the same value of the mean-free path and the Knudsen number is attained at higher pressure in helium. This means that the curve for helium should be shifted to the right, which corresponds to the experimental data in this figure.

C. Dependence on the particle size

At the same packing structure and the gas filling pores, the proportional increase in the particle size and the mean-free path keeps the value of the Knudsen number. As the mean-free path increases when the pressure decreases, the universal curve shifts to the left with increasing the particle size as shown in Fig. 12(b), which agrees with experiments.

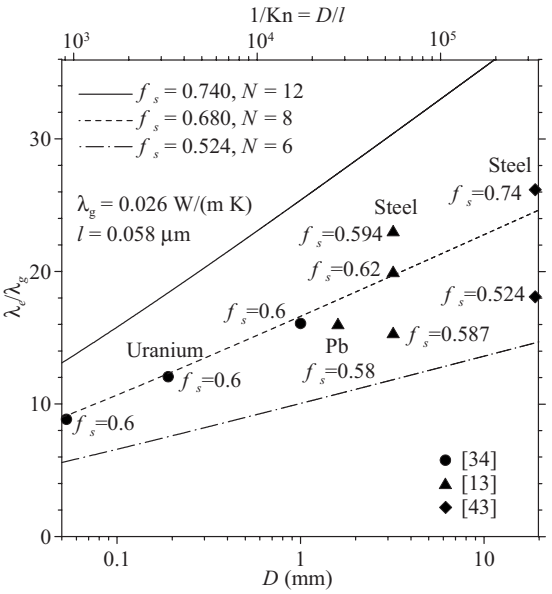

FIG. 13. Effective thermal conductivity λ_e of packed beds of metallic spheres in air at the normal conditions versus the diameter D. Curves show the approximation of isothermal spheres (41) with parameters f_s and N given in the upper left corner. Points show experimental data of Refs. 13, 34, and 43 with the indicated solid materials and values of f_s.

Figure 13 shows the data of different authors obtained in air at the normal conditions in a wide interval of the particle diameter D. The mean-free path $l=58$ is the same, so that the Knudsen number Kn is inversely proportional to D and the upper horizontal scale in this figure shows $1/Kn$. When D increases and Kn accordingly decreases, the contact resistance decreases (see Fig. 10) and the thermal conductivity given by Eq. (10) increases. The three curves in Fig. 13 are calculated in the approximation of isothermal spheres (41) with the parameters f_s and N corresponding to the fcc, bcc, and SC lattices (see Table I). The experimental points are obtained at different packing densities f_s, which complicates the analysis. Nevertheless, the general experimental tendency of increasing λ_e with D is evident. The experimental points for uranium[34] and lead[13] obtained at the density about $f_s=0,6$ lie near the middle dashed curve corresponding to bcc. In case of larger spheres, the variation in experimental data is greater but still in between the upper full (fcc) and the lower dash-dotted SC curves.

D. Peculiarities of powder beds

In the above experiments, even avec particles of few millimeters, the purely conductive regime of heat transfer in the gas phase is not attained despite extremely low values of the Knudsen number down to $Kn=10^{-5}$. The zone near the contact point between particles always contributes considerably, where the gas gap g is less or comparable with the mean-free

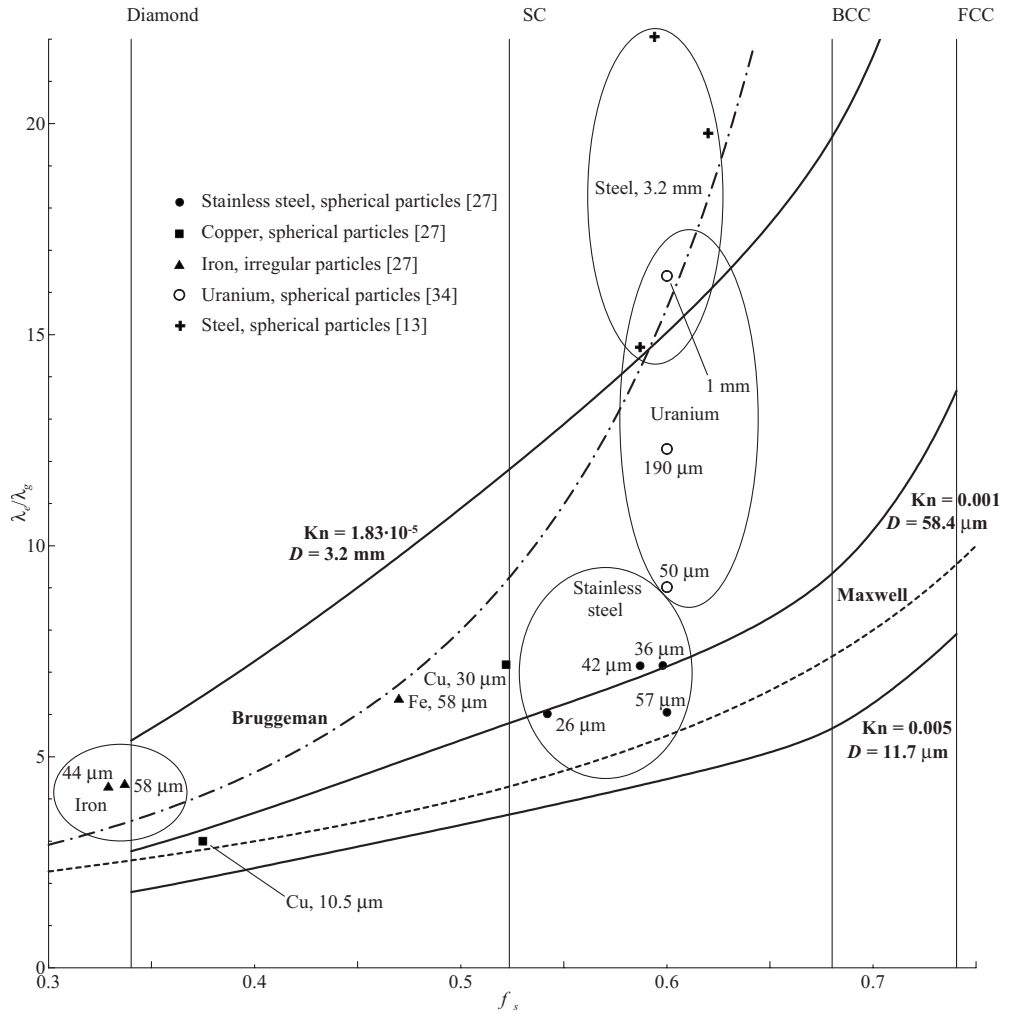

FIG. 14. Effective thermal conductivity λ_e of powder and packed beds in air at the normal conditions versus the volume fraction of solid f_s. Points show experimental data of Refs. 13, 27, and 34 with indicated material of the solid phase and the mean particle diameter. The shape of particles and the reference are given in the top left corner. The dashed curve shows the model of Maxwell (1) in the limit $\lambda_s/\lambda_g \to \infty$. The dash-dotted line shows the model of Bruggeman (2) in the same limit. Bold full lines show the approximation of isothermal spheres for the specified particle diameters D and the corresponding Knudsen numbers Kn. Thin vertical lines give the values of f_s for the regular structures are indicated on the top.

path l. Therefore, the considered problem includes the phenomena of rarefied gas even at the atmospheric pressure and macroscopic dimensions. The weight of these phenomena increases when the particle size decreases. Powder particles often have irregular shape, which complicates applying the model based on packed spheres. In addition, the volume fraction of solid f_s varies in a large range in powders.

Figure 14 shows the effective thermal conductivity versus the volumetric fraction of solid. Points indicate experimental data[13,27,34] obtained for powder and packed beds of metallic particles with high ratio λ_s/λ_g, when the conductivity of solid λ_s actually does not influence. Therefore, these data are compared with theoretical models in the limit $\lambda_s/\lambda_g \to \infty$. According to the models of Maxwell (1) and Bruggeman (2), the ratio is a function of f_s in the considered limit. The difference between these two models increases with f_s. The model of Maxwell better describes the micrometer-sized powders, while the model of Bruggeman tends to the millimeter-sized packed beds. The dependence on the particle size evident from the discussion in Sec. IV and III is neglected in these well-known models.

Bold full curves with the indicated values of D show the model proposed in this paper. The calculations are made in the approximation of isothermal spheres, which corresponds to the limit $\lambda_s/\lambda_g \to \infty$. First the values of λ_e/λ_g are evaluated for the regular structures from Table I corresponding to vertical thin lines in Fig. 14. Then these calculated points are connected by splines. These estimates correctly present the experimental dependencies on f_s and D. The model significantly underestimates the thermal conductivity for iron powder with irregular particles (triangles in Fig. 14) and copper powders (squares). In the first case, the discrepancy can arise because the particles are spherical in the model. In the second case, the oxidation of copper can influence the experimental result. Reference 27 points out that the two mentioned powders have wide size distributions. This also can be responsible for the disagreement with the model.

V. CONCLUSION

The model of discrete thermal resistances is proposed to take into account the strong thermal interaction between particles in powder and packed beds. This model applied to packed equal spheres estimates the effective thermal conductivity λ_e (10) as a function of the volume fraction of solid f_s, the mean coordination number N, and the thermal resistance of a contact between two neighbor particles Σ. Equation (10) is rigorous for regular packing with the lattices of Diamond, SC, bcc, and fcc and is applicable for random packing.

The problem of heat transfer in the domain of the contact between two particles includes conductivity in the solid phase of the particles and through a possible spot of the surface contact between them as well as heat transfer through the gap filled with gas where the conductive regime at greater distances from the center of the contact consecutively changes to the transition and free molecular regimes, while the distance to the center decreases. The intensity of heat transfer rapidly decreases with increasing the distance from the center where the gas gap is thin, so that the thickness of the gap is proposed to neglect. This assumption results in the model geometry of a nonideal thermal contact between half spaces. Then the heat transfer coefficient through the gas gap can be estimated by the well-known problem of heat transfer between parallel plates. The heat transfer in the solid phase is calculated in the two-dimensional cylindrical geometry.

The dimensional analysis for this model indicates that the contact resistance Σ depends on four dimensionless parameters: the relative size of the surface contact x, the ratio of thermal conductivities of the solid and gas phases λ_s/λ_g, the Knudsen number Kn, and the adiabatic exponent γ. The results of numerical calculation of this function are shown in Figs. 7, 8, and 10. In the case of small surface contacts ($0 < x \ll 1$) at high ratio λ_s/λ_g, the contact resistance is estimated by the model of circular contact between ideally insulated half spaces (35). Then the effective thermal conductivity is estimated by Eq. (36). The limits of application of this approximation and its precision are estimated by Fig. 7. For point contacts ($x=0$) at high λ_s/λ_g and not very small Kn, the approximation of isothermal spheres (39) works, which gives analytical formula for the effective thermal conductivity (41) with the limits of application estimated by Fig. 10.

The numerical calculations by the proposed model satisfactorily describe the experimental S-shaped curves of the effective thermal conductivity versus the logarithm of the gas pressure. The residual conductivity in vacuum is explained by a superposition of the radiative heat transfer and the transfer through small surface contacts between particles. The saturation at high pressures occurs because heat transfer is controlled by the solid phase. The proposed model also agrees with the experimentally observed variations in the S curves with changing the gas filling pores and the particle size.

The model explains the experimental tendencies of increasing the effective thermal conductivity with the particle size and the volume fraction of solid. It can be applied to powder beds with micron-sized particles as well as to packed beds with millimeter-sized particles. The discrepancy in the experimental data is explained by nonsphericity of the particles and their distributions in sizes not included in the model as well as by formation of small surface contacts between particles not controlled in the experiments.

The analysis of experimental data indicates that the free molecular and transition regimes of heat transfer in gas filling pores can be important even for millimeter-sized particles at the atmospheric pressure, when the Knudsen number is as low as $Kn=10^{-5}$. These phenomena specific for rarefied gases do define the complicated behavior of the considered media. The rigorous evaluation of the rarefied gas effects results in the model, which does not contain empirical parameters.

ACKNOWLEDGMENT

A.G. acknowledges the support of "Fondation CETIM."

*av.gusarov@relcom.ru

[1] S. Torquato, *Random Heterogeneous Materials* (Springer, New York, 2002).
[2] E.-B. Wei, G. Q. Gu, and Y. M. Poon, Phys. Rev. B **77**, 104204 (2008).
[3] L. Braginsky and V. Shklover, Phys. Rev. B **78**, 224205 (2008).
[4] A. V. Gusarov, I. Yadroitsev, Ph. Bertrand, and I. Smurov, ASME J. Heat Transfer **131**, 072101 (2009).
[5] G. K. Batchelor, R. W. O'Brien, Proc. R. Soc. London, Ser. A **355**, 313 (1977).
[6] W. D. Kingery, *Introduction to Ceramics* (Wiley, New York, 1976).
[7] X.-J. Hu, J.-H. Du, and S.-Y. Lei, B.-X. Wang, Int. J. Heat Mass Transfer **44**, 247 (2001).
[8] A. V. Luikov, *Heat and Mass Transfer. Handbook* (Energia, Moscow, 1971).
[9] A. V. Gusarov, T. Laoui, L. Froyen, and V. I. Titov, Int. J. Heat Mass Transfer **46**, 1103 (2003).
[10] J. C. Maxwell, *A Treatise on Electricity and Magnetism* (Dover, New York, 1954).
[11] D. A. G. Bruggeman, Ann. Phys. **416**, 636 (1935).
[12] R. E. Meredith and C. W. Tobias, J. Electrochem. Soc. **108**, 286 (1961).
[13] A. V. Luikov, A. G. Shashkov, L. L. Vasiliev, and Yu. E. Fraiman, Int. J. Heat Mass Transfer **11**, 117 (1968).
[14] Y. C. Chiew and E. Glandt, J. Colloid Interface Sci. **94**, 90 (1983).
[15] V. R. Raghavan and H. Martin, Chem. Eng. Process. **34**, 439 (1995).
[16] S.-Y. Lu, J. Appl. Phys. **85**, 264 (1999).
[17] C. Simovski and S. He, J. Appl. Phys. **86**, 3773 (1999).
[18] G. Gu and Z. Liu, J. Phys. D **25**, 249 (1992).
[19] C.-W. Nan, R. Birringer, D. R. Clarke, and H. Gleiter, J. Appl. Phys. **81**, 6692 (1997).

[20] S. Mercier, A. Molinari, and M. El Mouden, J. Appl. Phys. **87**, 3511 (2000).
[21] G. Q. Gu and K. W. Yu, J. Phys. D **30**, 1523 (1997).
[22] M. Grigoriu, J. Appl. Phys. **82**, 4346 (1997).
[23] S. Torquato, I. C. Kim, and D. Cule, J. Appl. Phys. **85**, 1560 (1999).
[24] S. Yagi and D. Kunii, AIChE J. **3**, 373 (1957).
[25] A. J. Slavin, F. A. Londry, and J. Harrison, Int. J. Heat Mass Transfer **43**, 2059 (2000).
[26] A. V. Gusarov, in *Rarefied Gas Dynamics*, edited by M. Capitelli, AIP Conf. Proc. No. 762 (AIP, New York, 2005), p. 294.
[27] M. Rombouts, L. Froyen, A. V. Gusarov, E. H. Bentefour, and C. Glorieux, J. Appl. Phys. **97**, 024905 (2005).
[28] W. W. M. Siu and S. H.-K. Lee, Int. J. Heat Mass Transfer **43**, 3917 (2000).
[29] W. W. M. Siu and S. H.-K. Lee, Int. J. Heat Mass Transfer **47**, 887 (2004).
[30] S. Kikuchi, Int. J. Heat Mass Transfer **44**, 1213 (2001).
[31] J. D. Albrecht, P. A. Knipp, and T. L. Reinecke, Phys. Rev. B **63**, 134303 (2001).
[32] J. H. Ferziger and H. G. Kaper, *Mathematical Theory of Transport Processes in Gases* (North-Holland, Amsterdam, 1972).
[33] R. G. Deissler and J. S. Boegli, Trans. ASME **80**, 1417 (1958).
[34] D. L. Swift, Int. J. Heat Mass Transfer **9**, 1061 (1966).
[35] S. K. Hsu and T. F. Morse, in *Rarefied Gas Dynamics*, edited by C. L. Brundin (Academic, New York, 1967), pp. 419–440.
[36] H. S. Carslaw and J. C. Jaeger, *Conduction of Heat in Solids* (Clarendon, Oxford, 1976).
[37] S. S. Sih, Ph. D. Thesis, University of Texas at Austin, 1996.
[38] I. V. Shishkovskii and N. L. Kupriyanov, High Temp. **35**, 710 (1997).
[39] T. H. C. Childs, C. Hauser, and M. Badrossamay, in *Proc. Institution of Mechanical Engineers B*, 219, 339 (2005).
[40] *Handbook of Physical Quantities*, edited by I. S. Grigoriev and E. Z. Meilikhov (CRC Press, Boca Raton, 1997).
[41] D. Baillis and J. F. Sacadura, J. Quant. Spectrosc. Radiat. Transf. **67**, 327 (2000).
[42] A. V. Gusarov and J.-P. Kruth, Int. J. Heat Mass Transfer **48**, 3423 (2005).
[43] G. Buonnano, A. Carotenuto, G. Giovinco, and N. Massarotti, ASME J. Heat Transfer **125**, 693 (2003).